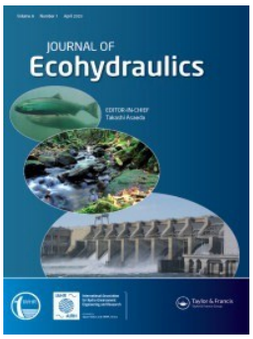

Journal of Ecohydraulics

ISSN: (Print) (Online) Journal homepage: https://www.tandfonline.com/loi/tjoe20

Evaluating Apple iPhone LiDAR measurements of topography and roughness elements in coarse bedded streams

Angel Monsalve, Elowyn M. Yager & Daniele Tonina

To cite this article: Angel Monsalve, Elowyn M. Yager & Daniele Tonina (2023): Evaluating Apple iPhone LiDAR measurements of topography and roughness elements in coarse bedded streams, Journal of Ecohydraulics, DOI: 10.1080/24705357.2023.2204087

To link to this article: https://doi.org/10.1080/24705357.2023.2204087

Published online: 23 Apr 2023.

JOURNAL OF ECOHYDRAULICS
https://doi.org/10.1080/24705357.2023.2204087

Evaluating Apple iPhone LiDAR measurements of topography and roughness elements in coarse bedded streams

Angel Monsalve, Elowyn M. Yager and Daniele Tonina

Center for Ecohydraulics Research, Department of Civil and Environmental Engineering, University of ID, Boise, ID, USA

ABSTRACT

High resolution topographic data are necessary to understand benthic habitat, quantify proc- esses at the water-sediment interface, and support computational fluid dynamics models for both surface and hyporheic hydraulics. In riverine systems, these data are typically collected using traditional surveying methods (total station, DGPS, etc.), airborne or terrestrial laser scanning, and photogrammetry. Recently, handheld surveying equipment has been rapidly acquiring popularity in part due to its processing capacity, price, size, and versatility. One such device is the iPhone LiDAR, which could have a good balance between precision and ease of use and is a potential replacement for conventional measuring tools. Here, we eval- uated the accuracy of the LiDAR sensor and a Structure from Motion (SfM) method based on photos collected using the iPhone Cameras. We compared the LiDAR and SfM elevations to those from a high-precision laser scanner for an experimental rough water-worked gravel- bed channel with boulder-like structures. We observed that both the LiDAR and SfM meth-
ods captured the overall streambed morphology and detected large (H_s 2 15 cm) and macro (5 cm < H_s < 15 cm) scales of topographic variations (H_s roughness). The

ARTICLE HISTORY
Received 5 January 2023
Accepted 29 March 2023

KEYWORDS
iPhone LiDAR;
Structure from motion;
Channel bed roughness

Introduction

Channel and floodplain topography is an essential input to hydraulic models that are vital for predicting realistic streamflow properties (Monsalve et al. 2017) and determining interactions between the bed and surface flow (Tonina and Jorde 2013). Accurate measurements of the topographic characteristics of riverine beds, including large, macro, and micro roughness (Figure 1b), are critical to construct these numerical flow models (Colombini and Stocchino 2005; Pokrajac et al. 2006; Roussinova et al. 2008; Kazemi et al. 2017; Lee 2018; Kuwata and Kawaguchi 2019; Dey et al. 2021; Kadivar et al. 2021). All computational fluid dynamics (CFD) models use the channel geometry to solve for the flow field in a given domain, resulting in a detailed description of flow variables that can vary in time and space such as velocity and forces (Tonina and Jorde 2013). In open channel flow, streambed top- ography can be described as the superimposition of several topographic features (Duffin et al. 2021), which span from large scale bed elevations gra- dients, like pool and bars (meters to hundreds of meters horizontal length scale), to local bed eleva- tion changes, like boulders and lateral expansions (tenths of a meter to a meter) (Figure 1). Whereas the large-scale topography defines the channel shape and streambed surface, the local bed elevation change controls the local roughness of the streambed surface. This roughness (Figure 1b) may include large-roughness elements, such as boulders, scour holes and depositional areas (~ decimeters to meter length scale, H_s), macro-roughness elements, like particle clusters (~ few centimeters to deci- meter) and micro-roughness elements, which are about the size of individual gravel grains in the riv- erbed (few millimeters to centimeters). As the spa- tial scale of a study decreases, the geometry of small elements or clusters of small elements, and their associated macro- and micro-roughness, becomes more and more important because it plays a key role in controlling turbulence properties and energy and momentum exchange within the entire fluid domain (Paola 1985; Antonia and Krogstad 2001; Poggi et al. 2003; Jim ́enez 2004; Leonardi et al. 2006; Schultz and Flack 2009; Doosttalab et al. 2016; Vanderwel and Ganapathisubramani 2019). The def- inition or magnitude of large, macro, or micro roughness varies depending on the study or field of study. For example, in river applications, macro- roughness elements are grains that rarely move in typical flow conditions, usually boulders (> 256 mm

CONTACT Angel Monsalve angelm@uidaho.edu Center for Ecohydraulics Research, Department of Civil and Environmental Engineering, University of Idaho, 322 E. Front St., Suite 340, Boise, ID 83702, USA

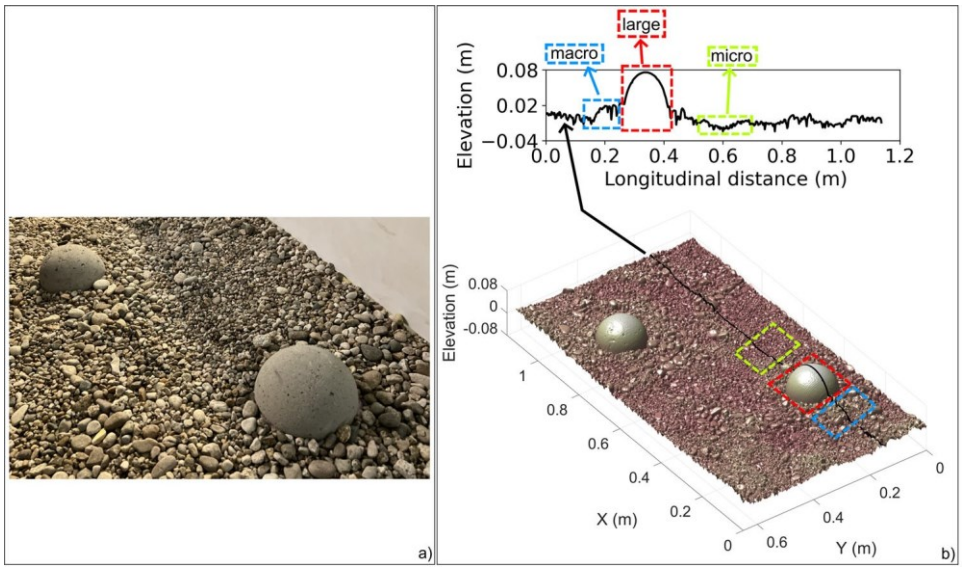

Figure 1. An example of the laboratory flume bed surface appearance and roughness scales. a) Photograph of the measured section in one of our experiments. Two boulders were included in this case. The perspective in this image helps identifying individual grains and their size relative to the boulders. b) DEM of the surface measured using a laser scanner. A similar per- spective to the photograph was used to compare details in figures a and b. Examples of the different scales of roughness that are present in our experiments are shown, which are superimposed on the large-scale topography of the simulated streambed.

in diameter) or the largest grain fractions (e.g. D_{84}, where the subscript represents the 84th percentile grain size) in the sediment bed (Canovaro and Solari 2007; Ferguson 2007; Nitsche et al. 2012; Schneider et al. 2015; Monsalve et al. 2017). However, in machining process, macro-roughness can be in the order of fractions of a millimeter (Kartal et al. 2017). In our case, the definitions of roughness scales are based on the sizes of our grain size distribution (GSD), boulders, and topographic features such as scour and deposition areas.

The recent development of handheld surveying equipment and digital photogrammetry has reduced the time, costs, and complexity associated with field campaigns and topographic measurements (Fonstad et al. 2013; Morgan et al. 2017; James et al. 2019; King et al. 2022; Tavani et al. 2022). For example, the Apple iPhone LiDAR is rapidly acquiring popu- larity for 3D representation of solid objects and sur- faces in part due to its processing capacity, price, size, and versatility (Luetzenburg et al. 2021) and Structure from Motion Multi-View Stereo (SfM) is rapidly becoming one of the most reliable alterna- tives for topographic surveys (Westoby et al. 2012; Carrivick et al. 2016; Smith et al. 2016; James et al. 2017; Marteau et al. 2017; Anderson et al. 2019; Kumar Karmacharya et al. 2019). Hereinafter, we refer to the Apple iPhone LiDAR as iPhone-LiDAR for simplicity.

When representing the measured surfaces both the iPhone-LiDAR and SfM methods can achieve a precision and accuracy of a few millimeters. The topographic surfaces generated by SfM are usually reported as being highly accurate (e.g. Fonstad et al. 2013; Javernick et al. 2014; Woodget et al. 2015; Carrivick et al. 2016; Marteau et al. 2017; Masteller and Finnegan 2017; Morgan et al. 2017; Pearson et al. 2017; Tabesh et al. 2019; Luetzenburg et al. 2021). The magnitudes of the elevation errors asso- ciated with SfM vary depending on the scale of the survey, but in general, they are in the range of mm to a few centimeters (Smith et al. 2016). In the case of the iPhone-LiDAR, given that the device has only been publicly available since 2020, there are fewer studies that have analyzed its accuracy, but reported errors as small as 6 mm when measuring snow depths (King et al. 2022) or ± 10 mm for small rect- angular objects (Luetzenburg et al. 2021; Tavani et al. 2022) have been reported. However, the accur- acy of the iPhone-LiDAR on the complex topogra- phies that commonly occur in river systems may differ from these values.

In this study, we evaluate the accuracy of the iPhone-LiDAR sensor to measure emergent (dry) rough gravel-bed channel topographies created in a laboratory flume that include boulder-like struc- tures, relatively flat but locally rough beds (micro- roughness), and scoured regions (macroroughness) (Figure 1). We also evaluate the accuracy of digital topographic surfaces constructed from photos col- lected using the iPhone Cameras and the Structure from Motion (SfM) method. We compare the iPhone-LiDAR and SfM derived topographic surfa- ces to those created using a high-precision laser scanner and analyze the sources, characteristics, and distribution of the residuals between the laser

scanned elevations and those of the two other tech- niques. We use a set of different and complemen- tary techniques to assess the accuracy of the iPhone- LiDAR and SfM to have a better understanding of the different type of errors that may be present when using the iPhone to collect data. Our methods include raster-to-raster and point-to-point compari- sons of bed surface elevations, and Fourier trans- form and power spectral density analyses of topographic profiles. Finally, a general description of cost-effectiveness when using the iPhone-LiDAR is provided to determine its applicability.

Methods

Laboratory experiments

We conducted two experiments that simulated the formation and evolution of bedforms in a mountain river at the Mountain StreamLab, University of Idaho (Budwig and Goodwin 2012). The experimen- tal configuration is based on the studies of Monsalve and Yager (2017) and Monsalve et al. (2017). Therefore, here we only focus on the most important similarities and differences. The setup is a simplification of a typical mountain river containing large roughness elements, represented by staggered concrete hemispheres. For simplicity, hereinafter, we refer to these elements as boulders. The boulders were 15.24 cm in diameter and were mounted over foam cylinders. The flume is 2 m wide and 20 m long but was partitioned with a wall to reduce the channel's width to 0.76 m and to create easier access to the test section from inside the flume. The test section was 8 m downstream of the upstream end of the flume to ensure fully developed turbulent flow before the first row of simulated boulders. The major difference in experimental conditions com- pared to Monsalve and Yager (2017) and Monsalve et al. (2017) is that we did not feed sediment at the upstream end of the flume. The initial bed consisted of a 30 cm thick sediment layer whose GSD ranged from 2 to 32 mm with a median grain size of 11 mm (D_{50}) and 5th, 16th, and 84th percentiles of 4.1, 5.9, and 19.8 mm, respectively. The longitudinal slope of our experiments was 2.7%, the bed started with a flat surface (except for the boulders) and we let it adjust to the imposed flow conditions (Table 1) until we visually observed that the bedforms were stable and practically no sediment was exiting the flume.

We conducted two experiments in which we var- ied the boulder spacing between experiments but held the flow discharge roughly constant (Table 1). We chose these two boulder spacings because it affects the flow field and controls the flow diver- gence around the boulders consequently it results in different topographies (e.g. scour and deposition characteristics) and therefore roughness. We meas- ured the bed topography and flow at the beginning (Initial, I) and end (Final, F) of each experiment to provide us four different topographies to test the iPhone-LiDAR and SfM.

Measurements

At the beginning and end of each experiment, in a representative area of the test section that included one boulder in Case1 and two boulders in Case2 (Table 1), we measured the bed topography using a high-speed laser displacement sensor, took photo- graphs from different angles for SfM photogram- metry, and scanned the bed with the iPhone-LiDAR using the Polycam software. We used a class II high-speed, high-accuracy CCD Laser Displacement Sensor model LK-G402 made by Keyence Corporation. This is a red semiconductor laser with wavelength of 655 nm, output power of 0.95 mW, and measuring range of about 20 cm. At reference distance (400 mm) it has a spot diameter of 0.29 mm and vertical accuracy of 0.1 mm. Hereinafter, we refer to this sensor simply as the laser. The laser was mounted on a motorized cart above the flume that was programmed to move at intervals of 1 mm in the horizontal plane (stopping for about 1 s at each location) and record the elevation data. Thus, the resolution of our laser observations is 1 mm x 1 mm. The elevation at a given location is the average of three individual measure- ments taken within the time the cart stopped at that place. All data were collected under dry bed condi- tions. For comparison purposes, these measurements will be considered the true elevation values.

We used the application 'Polycam' on an iPhone 13 Max Pro, operating system iOS 16, for our iPhone-LiDAR measurements. The technical capabilities of the iPhone-LiDAR are the same as the previous iPhone model (iPhone Pro 12 released in 2020) and are well described by Luetzenburg et al. (2021), and only the principal characteristics are mentioned here. The iPhone-LiDAR operates at wavelengths of 8XX nm, uses a Vertical Cavity Surface Emitting Lasers (or VCSELs) to emit the laser, and the direct time of flight of the pulses is measured with a Single Photon Avalanche Photodiodes (SPADs). The size and range (5 m) of the field of view (FoV) is constrained by flash illumination. A total of 576 points are emitted by the VCSEL when the device is activated. When measuring, Polycam displays a triangulated mesh over the object's surface while the iPhone is recording and pre-processing the elevations. As the user moves the device to collect more data, Polycam updates the

Table 1. Summary of the primary characteristics of the experiments and surface mesh generated by the iPhone-LiDAR and SfM.

Variable	Case1I	Case1F	Case2I	Case2F
Flow discharge (l/s)	57.3	57.3	57.0	57.0
Average flow depth (cm)	7.7	8.5	9.0	9.8
Boulder spacing (m)	0.762	0.762	0.61	0.61
Measured area (m^2)	0.252	0.293	0.717	0.786
Measured length (m)	0.630	0.620	1.138	1.209
Measured width (m)	0.400	0.472	0.630	0.650
Number vertices iPhone-LiDAR	14,858	12,067	17,580	20,897
Number faces iPhone-LiDAR	27,505	22,420	32,616	37,980
Resolution iPhone-LiDAR (mm)*	5.6	8.2	9.9	9.2
Number vertices SfM	157,196	189,409	318,775	335,597
Number faces SfM	314,209	378,559	637,198	670,882
Resolution SfM (mm)*	1.4	1.3	1.7	1.7
Number of photos SfM	261	285	589	197

*Approximate resolution based on the average edge length of the triangulated irregular mesh.

mesh in real-time and shows the areas that are effectively measured and those outside the FoV in different colors. These features allow the user to identify zones that could have been missed or that need additional scans. The iPhone 13 Pro models are equipped with a barometer, three-axis gyroscope, and accelerometer, which are used by Polycam to determine the three spatial coordinates of the meas- ured surfaces. The software post-process the data directly on the iPhone and the results can be exported in different mesh and point cloud formats. In all cases we used ".obj" format. We further post-processed the data using the open-source system MeshLab for processing and editing 3D irregular tri- angular meshes (available in meshlab.net) to reduce the scan to only the region of analysis and visualize the results. No filtering, cleaning, scaling, or remeshing was conducted. The average resolution of the iPhone-LiDAR surfaces was between 5.6 and 9.9 mm (Table 1).

We used the iPhone cameras to take photographs of the studied area and reconstruct the bed topog- raphy using SfM photogrammetry using AgiSoft Metashape Professional, version 1.8.4. We used the wide camera, which has a 12 MP resolution with f/1.5 aperture and focal length of 6 mm. All our measurements were collected using the automatic mode, resulting in exposure times approximately between 1/40 to 1/60 s. We worked in an indoor environment using artificial diffuse lightning. Thus, the illumination was consistent for all of the photo- graphs and the different study cases. SfM techniques and theory has been described in great detail in other studies (e.g. Fonstad et al. 2013; Javernick et al. 2014; Woodget et al. 2015; Carrivick et al. 2016; Masteller and Finnegan 2017; Morgan et al. 2017; Luetzenburg et al. 2021), therefore, we only mention the characteristics and properties of the data collected. Given that we were working over a relatively small area and had access to the study zone from all directions, our photographs over- lapped more than 90%, which is higher than the 80% forwards and 60% sidewards recommended by AgiSoft. In each case we used all the collected pho- tos, but we disabled and excluded from photogram- metric processing those images with quality value lower than 0.5 units as suggested by AgiSoft. Thus, the final number of photos used in each case was variable (Table 1). To scale and reference the gener- ated cloud points, we placed six control points, three at the upstream and three at the downstream end of the measurement area and measured their locations using the laser. Additionally, we identified reference points that are common in different images to help the software with photo alignment. In average the resolution of the SfM irregular tri- angle meshes was approximately 1 mm (Table 1).

Evaluation of differences in elevation

After post-processing the iPhone-LiDAR and SfM data, we obtained 3D representations of the topog- raphy in Wavefront .obj format that contained the coordinates, texture (color), and normals of each vertex and the faces that make each polygon of an irregular triangular mesh. This geometrical represen- tation allowed us to compare surfaces with different resolutions and extract differences in elevations at any location within the study zone.

For a general evaluation of the ability of the iPhone-LiDAR and SfM to capture topography and roughness elements in gravel bed channels, we com- pared the generated surface elevations to the laser observations using a raster-to-raster approach. In this case all surfaces were mapped onto a 1 × 1 mm uniform mesh to create a Digital Elevation Model (DEM) and differences in elevations were evaluated using a DEM of Difference (DoD). We quantified the residuals or errors as the difference in elevations ($Dz_i = z_j - z_l$ where the subscript j corresponds to the laser and l to the iPhone-LiDAR or SfM method) at each vertex (i). Then, we calculated the mean absolute error (MAE, Eq. 1), mean (Dz, Eq. 2) and standard deviation (r_{Dz}, Eq. 3) of the

residuals to determine the accuracy and precision of the surface representations of the iPhone-LiDAR and SfM:

$$MAE = \frac{\sum_{i=1}^{n} |\Delta z_i|}{n} \quad \text{Eq. 1}$$

$$\bar{\Delta z} = \frac{\sum_{i=1}^{n} \Delta z_i}{n} \quad \text{Eq. 2}$$

$$r_{\Delta z} = \sqrt{\frac{\sum_{i=1}^{n} (\Delta z_i - \bar{\Delta z})^2}{n}} \quad \text{Eq. 3}$$

where n is the total number of vertices in a DEM.

We also explored the characteristics of Δz_i between the laser scan and the iPhone-LiDAR or SfM using a point-to-point approach. In this case, we compared the elevation of each vertex of the generated surfaces with that of the closest point of the laser scan in terms of horizontal distance. Compared to the raster-to-raster approach this method does not depend on data interpolation, therefore, it helped us to characterize how the sim- plifications of surface features of the iPhone-LiDAR and SfM methods affected the errors. In this case, when the vertex of the iPhone-LiDAR or SfM sur- face contains a point that is a short distance away from a point in the laser scan, Δz_i between these two points effectively measures the difference between the two methods because the two points are at about the same horizontal location. But, as the distance between the laser and corresponding SfM/iPhone-LiDAR point increases, a portion of Δz_i is due to a true elevation difference because the 2 points are measuring different locations. The resid- ual's (Δz_iÞ distribution and standard deviation could therefore be used as an indicator of how much the surface obtained using the iPhone-LiDAR or SfM was simplified.

Surface roughness simplifications

We cannot determine the iPhone-LiDAR resolution of captured roughness elements only using the iPhone-LiDAR technical specifications . Luetzenburg et al. (2021) determined an accuracy and error in precision of 1 cm when measuring objects with side length larger than 10 cm. However, these values were obtained based on the length, width, and height of isolated objects and not on continuous rough surfaces. We expanded their analysis by eval- uating different roughness scales, including macro- and micro-roughness, of our scanned beds to deter- mine the size of the surface features that were prop- erly captured. We applied fast Fourier transform (FFT) and power spectral density estimation (SDE) based on the Welch's method on extracted longitu-dinal profiles from our scans to explore what rough- ness components were similar and different between the laser scan, iPhone-LiDAR, and SfM. We used Delaunay triangulations with linear interpolations to sample the iPhone-LiDAR and SfM surfaces at equally spaced locations (1 mm resolution) to apply the FFT and

Results

General characteristics of the processed digital surfaces

At a resolution of 1 mm x 1 mm, the laser scan was able to capture the texture of the sediment beds in detail (Figure 1). Even small features such as imper- fections in the boulders, noticeable as black/dark grey holes in the photo (Figure 1a) and in digital reconstruction (Figure 1b), were present in the laser data. In general, the laser data had little noise or erroneous measurements. We removed less than 0.5% of the points, which were easily identifiable because the laser output file registered them as hav- ing an elevation of −0.99 m. We observed that all the registered errors were associated with points where the laser spot was not precisely focused on a single location, such as at the edge of a grain.

The iPhone-LiDAR was able to accurately capture the most distinct topographical features in all cases. For example, it correctly measured the overall shape and dimensions of the boulders, relatively flat regions, and scour and deposition zones (Figure 2). However, small roughness elements, such as small individual grains, were omitted in the surface repre- sentation. Therefore, all surfaces created using the iPhone-LiDAR data appear to be a smoothened ver- sion of the laser scan. The threshold grain size that can be measured by the iPhone-LiDAR will be dis- cussed in the next section. The surfaces generated using SfM display great resemblance to those meas- ured with the laser, even the size, location, and orientation of small grains are well represented (Figure 2).

Differences in elevation using raster comparisons

The iPhone-LiDAR/laser DOD residual means (Figure 3) were close to zero in all cases (Table 2), with a maximum $\bar{\Delta z}$ of 0.65 mm for Case1I. These small means (Table 2) confirm negligible bias or systematic errors in the iPhone-LiDAR surfaces and that most of the error is effectively random error described by the standard deviation of the residuals ($r_{\Delta z}$, Eq. 3). For simplicity and to provide a gener- ally applicable example, we focus on Case2F to graphically display and explain all the results.

The standard deviation of the errors for the 1 x 1 mm grid comparison was between 3.24 and

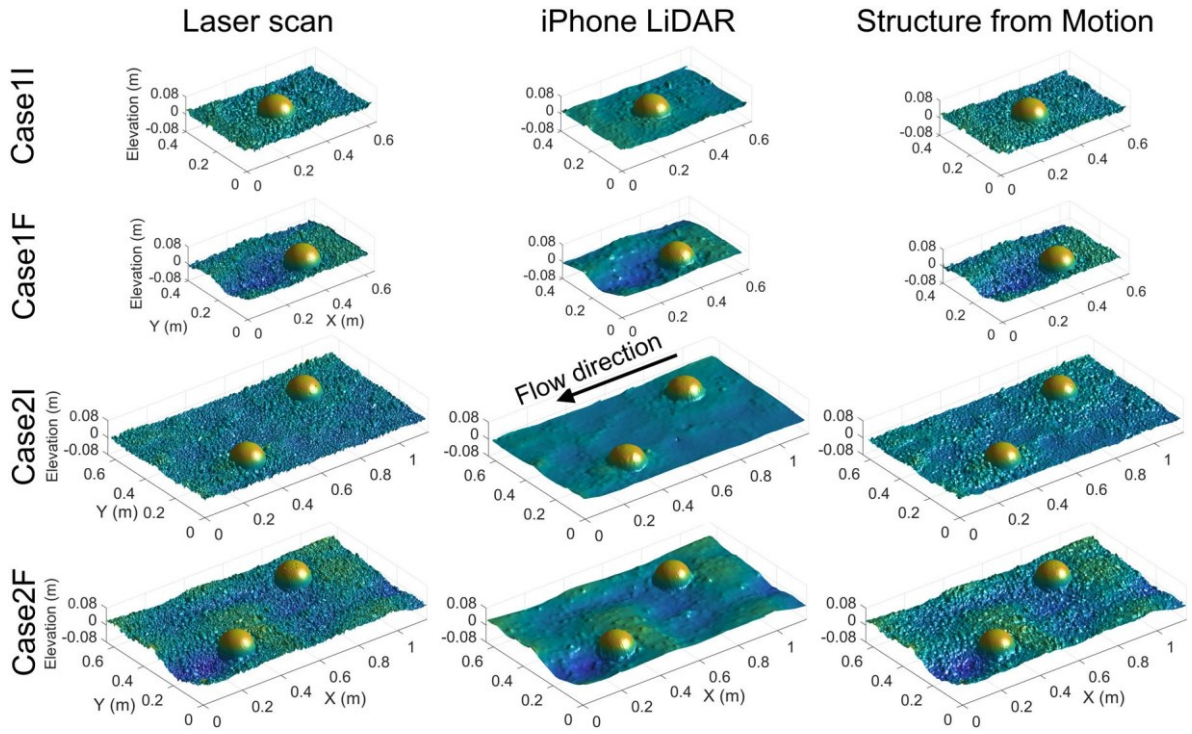

Figure 2. Bed surface elevations measured (laser scan) and generated (iPhone-LiDAR and SfM) for each case. Different meth- ods are display in columns and cases in rows. Flow direction is from right to left. Surfaces are colored by elevation. In the fig- ure, we used blue and green shades of color to highlight scoured and deposited areas, respectively. The color scale is only a reference as some of the boulder's edges appear colored as green.

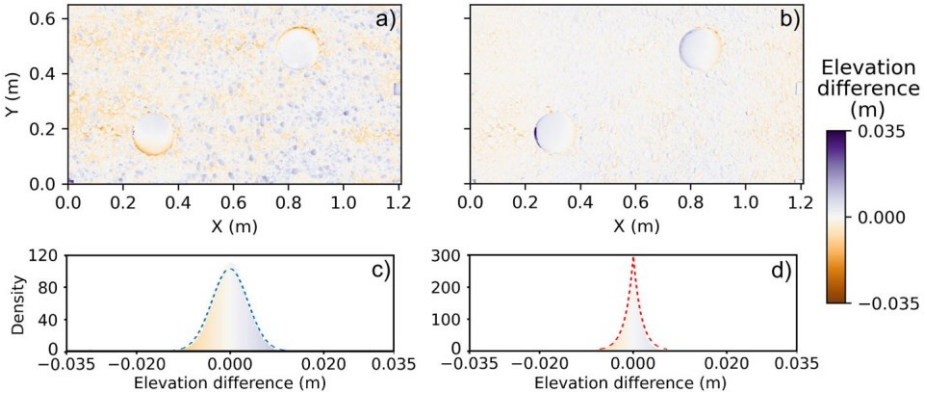

Figure 3. Differences in elevations (or DoD) in Case2F between the surfaces generated by the laser scan and those from the
a) iPhone-LiDAR and b) SfM. These DoD had a 1 mm resolution. A positive value indicates that the measured elevation (laser) was higher than that obtained using the iPhone-LiDAR or SfM. The distribution of the residuals for the c) iPhone-LiDAR and d) SfM is colored using the same color scale to highlight magnitude and density. Segmented lines represent fits to a normal dis- tribution in c) and a Laplacian distribution in d).

Table 2. Characteristics of the errors when comparing the measured elevations using the laser scan to those generated by the iPhone-LiDAR and SfM. For this raster comparison, two DoD resolutions were used for sensitivity analysis with 1 mm corresponding to the laser scan and other values to the iPhone-LiDAR resolution in each case.

		Average error ($\bar{D}_z$, mm) (*MAE*, mm)		Error standard deviation (r_{Dz}, mm)		Mean absolute error	
Topography used	DEM Resolution (mm)	iPhone-LiDAR	SfM	iPhone-LiDAR	SfM	iPhone-LiDAR	SfM
Case1I	1.0	−0.65	0.39	3.24	3.16	2.47	2.18
Case1F	1.0	0.09	0.12	3.58	1.90	2.77	1.21
Case2I	1.0	−0.11	0.13	4.26	2.12	3.25	1.56
Case2F	1.0	−0.07	−0.01	3.83	2.40	2.98	1.64
Case1I	5.6	−0.67	0.38	3.25	3.19	2.47	2.20
Case1F	8.2	0.07	0.03	3.57	2.33	2.75	1.29
Case2I	9.9	−0.10	0.14	4.32	2.24	3.30	1.61
Case2F	9.2	−0.10	−0.03	3.83	2.33	2.96	1.63

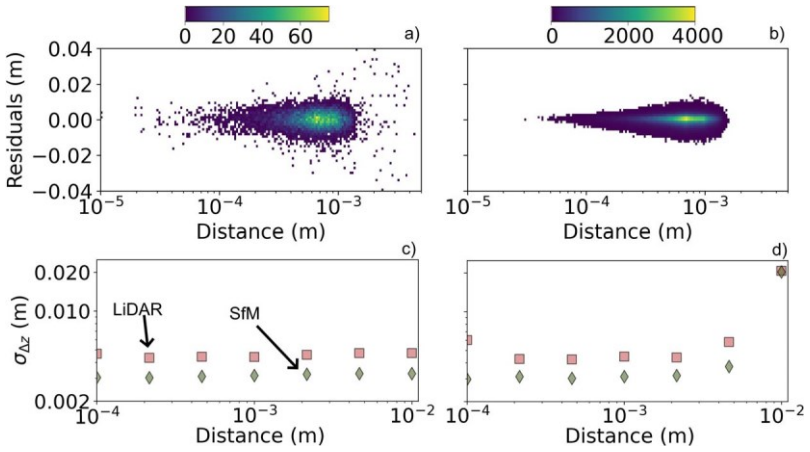

Figure 4. Distribution of differences in elevation using a point-to-point approach in Case2F comparing the laser scan to the surfaces generated by the a) iPhone-LiDAR and b) SfM. The residuals are colored by point counts (color bar) to highlight the location of points at different distances between the laser scan and the iPhone-LiDAR/SfM. The variability in r_{Dz} considering
c) cumulative distances and d) individual intervals. Given that we colored the residuals by count number some individual points at a distance longer than 2 mm are not clearly visible in b).

4.26 mm for the iPhone-LiDAR and 1.9 and
3.16 mm for SfM (Table 2). In all cases r_{Dz} and MAE were smaller for the SfM compared to the iPhone-LiDAR. These r_{Dz} are similar in size to the smallest grain size fractions on the bed, e.g. D_5 ¼
4.1 mm, but r_{Dz} does not represent the size of the smallest captured grains. We analyzed the depend- ency of these results to the selected 1 x 1 mm grid size by calculating Dz and r_{Dz} on DEMs with the iPhone-LiDAR resolution (a coarser grid). We observed that the estimated r_{Dz} remained practically constant when we coarsened the DoD resolution (changes < 0.5 mm) indicating that our results and analysis are valid at the spatial scale on which we are working.

The spatial distribution and magnitude of errors represented in the DoD also show no systematic errors and suggests that most of the elevations dif- ferences stem from simplifications or smoothening of the surfaces and removal of the micro roughness (Figure 3). For example, the shape of individual grains can be observed in the iPhone-LiDAR DoD (Figure 3a) as an orange or purple (extreme values in the color bar) colored surface indicating that those grains were not captured by this technique. In contrast, the outlines of single grains are observed in the SfM DoD (Figure 3b). This observation sug- gests that the SfM method simplifies the grain edges, but the general shape is well represented. In both the iPhone-LiDAR and SfM, the largest errors were located at the base of the boulders where an abrupt change in elevation occurs.

The differences in r_{Dz} between the iPhone-
LiDAR and SfM can be furthered compared using the distributions of errors for each method (Figure 3c and d). The distribution of errors for the iPhone- LiDAR is broader (Figure 3c, larger r_{Dz}) compared to the SfM (Figure 3d, smaller r_{Dz}). In terms of

magnitude, 98.65% and 99.53% of all the elevation differences were within an error of ±0.01 cm for the iPhone-LiDAR (Figure 3c) and SfM, respectively (Figure 3d). These differences in r_{Dz} could be con- sidered small, but they have an important impact on the probability distribution that describes the error characteristics. To analyze if the residuals follow a certain distribution we used the Kolmogorov- Smirnov (K-S) goodness-of-fit test (95% confi- dence). The K-S tests the null hypothesis that the residuals in the iPhone-LiDAR come from a stand- ard normal distribution (Figure 3c) and in the SfM come from a Laplace distribution (Figure 3d), against the alternative that the residuals do not come from such distributions. The p value of both K-S tests was larger than 0.05 for both techniques, thus we cannot reject the null hypothesis and sug- gests that these distributions are good approxima- tions of the actual residual distributions.

Differences in elevation using point to point comparisons

The spatial distribution of the residuals considering a point-to-point approach complements the distri- butions of residuals from the raster analysis. Most of the iPhone-LiDAR and SfM surfaces have a cor- responding point at a distance of 0.7 mm from the points in the laser data (yellow region in Figure 4a and b). This small distance, relative to the GSD of the bed, suggest that both the iPhone-LiDAR and SfM are likely measuring the same grain or bed fea- ture as the laser. As the distance increases between points on the laser and closest corresponding points on the iPhone-LiDAR/SfM, more scatter around the mean (i.e. residual practically equals to zero) was observed (Figure 4a and b), especially for the iPhone-LiDAR where individual points start to

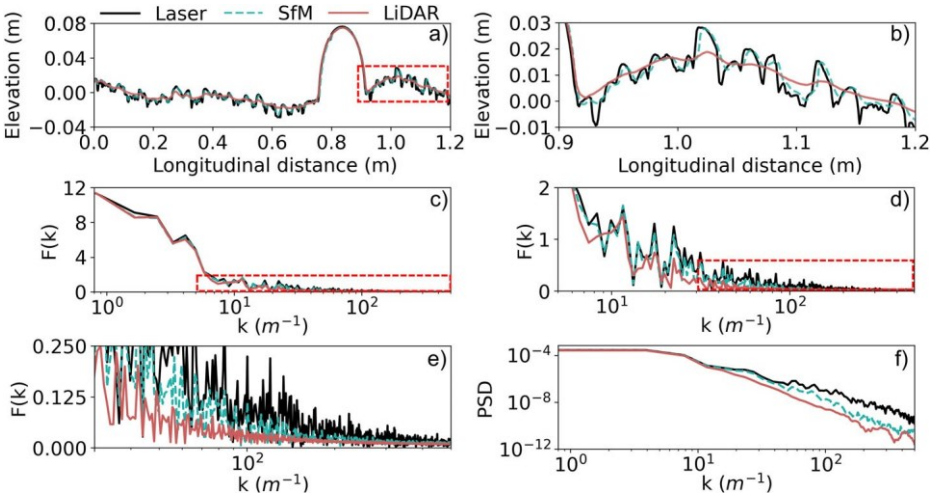

Figure 5. Bed surface elevation profile and analysis of its signal. a) Longitudinal profile along one of the boulders in Case2F extracted from the measured (laser scan) and generated surfaces (iPhone-LiDAR and SfM). The red segmented area is dis- played in b). b) A detailed view of the generated bed surface elevations. c) Fourier transform of the profile shown in a). d) An enlarged view of the red segmented area in c). e) An enlarged view of the red segmented area in d). f) Power spectral density of the profile shown in a).

disperse relatively far from the zone that represents a residual of 0 m. The increase in the residual mag- nitude with larger distance (Figure 4a and b) between corresponding points suggests that the points are sampling different bed features or that the SfM/iPhone-LiDAR couldn't capture the actual surface elevation at that given location.

We also analyzed how the distance between points on the laser and closest corresponding points on the iPhone-LiDAR/SfM affects the variability in r_{Dz}: We considered two cases: cumulative distance and individual intervals. Cumulative distance means that, for example, at a distance of 10^{-3} m all points between 10^{-5} and 10^{-3} m are considered in the r_{Dz} calculation, being 10^{-5} the smallest observed dis- tance between a laser observation and the corre- sponding iPhone-LiDAR/SfM point. Individual intervals indicate that r_{Dz} is calculated for only one distance interval at a time. In this case, evenly spaced distance values on a logarithmic scale were used. For example, between 10^{-4} and $2.154\text{-}10^{-4}$ m, then $2.154\text{-}10^{-4}$ to $4.641\text{-}10^{-4}$ m and so forth. When considering increasingly longer cumulative distances between corresponding points, r_{Dz} remains almost constant for the iPhone-LiDAR and SfM methods (Figure 4c). This is because although the dispersion of the residuals of the corresponding points increases, the number of points around the mean residual value (residual of ~0 m approxi- mately) also increases, thus maintaining r_{Dz}: If intervals of distances between corresponding points are instead considered (Figure 4d), r_{Dz} magnitudes are similar to those calculated using cumulative dis- tances up to 2 mm. Then, for longer distances, r_{Dz} increases reaching a value of ~2 cm at a distance of 1 cm. This suggest that in the coarser areas of the mesh both methods, iPhone-LiDAR and SfM, fail the accurately represent the true elevation of the surface. Similar to the DoD calculations, in the point-to-point approach the r_{Dz} of the SfM is smaller than that of the iPhone-LiDAR (Figure 4c and d), but is about 1 mm larger than that calcu- lated using DoD in both cases.

Simplifications of small-scale roughness

When comparing the surfaces generated by the iPhone-LiDAR to those measured by the laser scan it can be observed that the smallest grains and the small-scale features tend to disappear resulting in a relatively smooth surface (Figure 2). The SfM surfa- ces closely resemble those of the laser scan, but some details are also lost (Figure 3b). The iPhone- LiDAR and SfM methods can accurately capture the bedform heterogeneity and large- and macro-rough- ness elements, for instance, the boulder and the regions of scour and deposition (Figure 5a). However, when analyzing at the smaller scale of micro-roughness elements (Figure 5b), the charac- teristics of the smoothening can be evaluated. The iPhone-LiDAR profile maps the general surface of the bed but removes some elevation heterogeneity, simplifying the topography along the mean elevation of the fine scale roughness (Figure 5b). In the SfM profile, the elevations of individual fine scale rough- ness peaks are well characterized, but the corre- sponding valleys were smoothened. At this small spatial scale, the SfM method seems to fail in repro- ducing the sharp gradients that can be found at the grain's edges, which can be seen as an apparent off- set (towards the right in this case) of the surface ele- vations. Still, the SfM surface generally captures the

detailed form and large- and macro-roughness of our beds (Figure 5b). Using the Fourier transforms and power spectral density analysis we estimated the sizes of the features that were captured in the differ- ent methods. All signals seem to have a similar Fourier transform, which can be visually identified considering the coefficients in the Fourier transform ($F\eth k\text{Þ}$) in Figure 5c, especially up to approximately frequency k ¼ 20 $\mathbf{m}^{-1}$, equivalent to a feature size of 5 cm (Figure 5d). Then, from k ¼ 20 $\mathbf{m}^{-1}$ to 100 $\mathbf{m}^{-1}$ the iPhone-LiDAR's Fourier transform departs from that of the laser scan, suggesting that the smoothening of the bed surface occurs for grains sizes between 5 cm and 1 cm. For k larger than 100 $\mathbf{m}^{-1}$ the Fourier transform is practically zero suggesting that features smaller than 1 cm are not mapped by the iPhone-LiDAR (Figure 5d). In the case of the SfM the Fourier transform is similar to that of the laser scan up to approximately k ¼ 60 $\mathbf{m}^{-1}$, equivalent to a feature size of 1.67 cm (Figure 5e). Then, nearly from k ¼ 60 $\mathbf{m}^{-1}$ to 400 $\mathbf{m}^{-1}$ the SfM's Fourier transform appears to have smaller coefficients, which suggests that grain sizes between 0.25 to 1.67 cm are smoothened. For frequencies larger than 400 $\mathbf{m}^{-1}$, the coefficients are almost zero suggesting that SfM does not capture features smaller than 0.25 cm (Figure 5e).

The power spectral density (PSD) analysis is a complementary method that helps interpretation what was shown using Fourier transforms. All PSD signals overlapped up to approximately k ¼ 20 $\mathbf{m}^{-1}$ (Figure 5f). For $20 < k < 100$ $\mathbf{m}^{-1}$ the iPhone-LiDAR's PSD decreases at a higher rate than the laser and SfM PSD. This is the spatial region where surface smoothening occurs. For $k > 100$ $\mathbf{m}^{-1}$ the iPhone-LiDAR PSD seems to maintain the slope with frequency of the previous region, but oscillates and has noise around that overall slope, which may suggest that those PSD values are beyond the meth- od's capturing capabilities. The SfM PSD overlaps with the laser scan PSD up to approximately k ¼ 60 $\mathbf{m}^{-1}$ (Figure 5f). Then, for $60 < k < 400$ $\mathbf{m}^{-1}$ the SfM PSD departs from the laser PSD and decreases at a higher rate. This may explain why some valleys and small grains are smoothened by this method (Figure 5b).

Discussion

Our analysis the surfaces generated using the iPhone-LiDAR and SfM revealed that both methods can accurately capture the general form and large- and macro-roughness of bed surfaces at the spatial scale of the elements of our experiments (mm to tens of cm). Furthermore, the SfM method can include small scale elements, thus accounting for small scale bed roughness. This is reflected in $\overline{Dz}$, which is negligible, and r_{Dz} where the iPhone-LiDAR and SfM have values below 4.3 and 3.2 mm, respectively (Table 2), which are close to the 5th per- centile of the GSD, D_5 ¼ 4.1 mm. However, the properties of the residuals and the sources of these errors as well as the advantages and disadvantages of each method need to be considered when select- ing a method for practical applications.

In our case, iPhone-LiDAR, collecting, process- ing, and post-processing data with the iPhone was faster and easier than with the SfM from a user's perspective. As a reference, scanning the bed of Case2F using Polycam took us about 3 min and processing the data ~8 min. In the case of SfM, tak- ing the almost 200 photos took about 25 min, but processing the data, including loading and referenc- ing the images and creating the surfaces, took us about 24 h. The interface of Polycam, with its real- time update of the scanned surface and relatively fast processing, allows someone to examine the results immediately with the possibility of amending problems before leaving the location. The iPhone- LiDAR requires practically no configuration when scanning. The mesh resolution and vertex locations are determined automatically by the Polycam. Local adjustments of the generated surface are also defined by the software when an object is scanned from different angles. Although having the software determine all the mesh parameters may result in an easier use of the technique in most cases, not having the ability to configure the acquisition parameters could lead to problems in capturing a desired bed feature.

The simplification or smoothening of the surfaces may be one drawback of the iPhone-LiDAR com- pared to SfM. Grains between 1 and 5 cm are sim- plified by the iPhone-LiDAR, thus affecting the representation of surface roughness. However, losing this scale of roughness may not be a practical prob- lem when modeling open channel flow with two dimensional, 2D, models. In these models, the mesh usually includes the general geometry or shape of a channel and the most relevant topographic features such as large boulders or cobble clusters, but, local roughness is parametrized using a roughness coeffi- cient (Tonina and Jorde 2013). On the other hand, modeling small-scale turbulence processes in a 3D flow model using a smoothened surface may intro- duce errors because boundary layers are poorly rep- resented (Kadivar et al. 2021).

An advantage of the SfM over the laser is the possibility of capturing areas of the bed that are hid- den in a plan view perspective, especially around pockets of grains. Some areas were not reached because the laser could be operated only from a

direction perpendicular to the bed surface. However, changing locations and angles allowed the cameras and our SfM-generated surface to capture these pla- ces. These unmeasured areas could be a source of error in our analysis, but we did not have a method to directly measure the elevation of such small places.

In our study, the elevation errors of the iPhone-LiDAR surfaces are smaller than previously reported. For example, Luetzenburg et al. (2021) reached an accuracy of 1 cm when measuring small objects and King et al. (2022) reported an RMSE of 6 mm in snow depth measurements. In our case, given that our systems are not biased, the RMSE is equivalent to r_{Dz} and had average values close to
3.7 mm. This can be considered a relatively small magnitude and an accurate result considering that the laser scan had a resolution of 1 x 1 mm and the smallest grains in the bed were only 2 mm in size. We based our Fourier transform and Power Spectral analysis on visual interpretations and we are aware that the defined k ranges could be slightly different but this would have a limited impact on our result interpretation.

Conclusion

We analyzed the accuracy of surfaces produced using the iPhone iPhone-LiDAR and SfM compared to a high precision laser scan. The iPhone-LiDAR-generated surfaces accurately represented the large- scale bed elevation variability and macro-roughness in our experimental cases. However, micro rough- ness elements, e.g. small grains present in the bed grain size distribution, were not mapped, resulting in a smoother bed surface than that mapped by the laser scan. Although the removal of micro bed fea- tures may be considered a problem in some cases, it must be evaluated relative to the scale of a particular study. Studies where the main bed features are larger than 5 cm, the threshold below which the iPhone-LiDAR starts simplifying the elements, can use this tool to obtain a reliable surface representa- tion. On the other hand, if accurate estimates of the small-scale structure of turbulence are needed from a numerical model that uses the bed surface, a good representation of this surface micro roughness is required and the iPhone-LiDAR would not be an appropriate instrument to measure the bed surface. SfM, on the other hand, was consistently more accurate than the iPhone-LiDAR and it was able to capture even the smallest grains present in the bed. However, it involved a relatively more complex workflow. In practical applications, we recommend evaluating the cost-effectiveness of both methods and to decide on the method depending on the roughness resolution needed, time availability for producing and evaluating the generated surfaces, and the spatial range of application.

Disclosure statement

No potential conflict of interest was reported by the authors.

Funding

This research was partially supported by National Science Foundation 2100926 grant.

ORCID

Angel Monsalve http://orcid.org/0000-0002-7369-1602

References

Anderson K, Westoby MJ, James MR. 2019. Low-budget topographic surveying comes of age: structure from motion photogrammetry in geography and the geo-sciences. Prog Phys Geogr. 43(2):163–173.

Antonia RA, Krogstad P. 2001. Turbulence structure in boundary layers over different types of surface rough-
ness. Fluid Dyn Res. 28(2):139–157.

Budwig RS, Goodwin P. 2012. The center for ecohydraulics research mountain stream lab – a facility for collabora- tive research and education. In: Aung W, editor. Innovations 2012: world innovations in engineering edu- cation and research. Potomac (MD): iNEER; p. 17–28.

Canovaro F, Solari L. 2007. Dissipative analogies between
a schematic macro-roughness arrangement and step-pool morphology. Earth Surf Process Landforms. 32(11):1628–1640.

Carrivick JL, Smith MW, Quincey DJ. 2016. Structure from motion in the geosciences. 1st ed. Oxford, UK: Wiley-Blackwell.

Colombini M, Stocchino A. 2005. Coupling or decoupling bed and flow dynamics: fast and slow sediment waves at high Froude numbers. Phys Fluids. 17(3):036602.

Dey S, Rathore V, Penna N, Gaudio R. 2021. Hydrodynamics of flow over a gradually varied bed roughness. Phys Fluids. 33(12):125112.

Doosttalab A, Araya G, Newman J, Adrian RJ, Jansen K, Castillo L. 2016. Effect of small roughness elements on thermal statistics of a turbulent boundary layer at mod- erate Reynolds number. J Fluid Mech. 787:84–115.

Duffin J, Carmichael RA, Yager EM, Benjankar R, Tonina D. 2021. Detecting multi-scale riverine topographic variabil- ity and its influence on Chinook salmon habitat selection. Earth Surf Process Landforms. 46(5):1026–1040.

Ferguson R. 2007. Flow resistance equations for gravel- and boulder-bed streams. Water Resour Res. 43(5): W05427.

Fonstad MA, Dietrich JT, Courville BC, Jensen JL, Carbonneau PE. 2013. Topographic structure from motion: a new development in photogrammetric meas- urement. Earth Surf Process Landforms. 38(4):421–430. James MR, Chandler JH, Eltner A, Fraser C, Miller PE, Mills JP, Noble T, Robson S, Lane SN. 2019. Guidelines on the use of structure-from-motion

photogrammetry in geomorphic research. Earth Surf Process Landforms. 44(10):2081–2084.
James MR, Robson S, d'Oleire-Oltmanns S, Niethammer U. 2017. Optimising UAV topographic surveys processed with structure-from-motion: ground control qual- ity, quantity and bundle adjustment. Geomorphology. 280:51–66.
Javernick L, Brasington J, Caruso B. 2014. Modeling the topography of shallow braided rivers using structure-from-motion photogrammetry. Geomorphology. 213: 166–182.
Jim ́enez J. 2004. Turbulent flows over rough walls. Annu Rev Fluid Mech. 36(1):173–196.
Kadivar M, Tormey D, McGranaghan G. 2021. A review on turbulent flow over rough surfaces: fundamentals and theories. Int J Thermofluids. 10:100077.
Kartal F, Yerlikaya Z, G∈okkaya H. 2017. Effects of machining parameters on surface roughness and macro surface characteristics when the machining of Al-6082 T6 alloy using AWJT. Measurement: J Int Measurement Confederation. 95:216–222.
Kazemi E, Nichols A, Tait S, Shao S. 2017. SPH model- ling of depth-limited turbulent open channel flows over rough. Int J Numer Methods Fluids. 83(1):3–27.
King F, Kelly R, Fletcher CG. 2022. Evaluation of LiDAR-derived snow depth estimates from the iPhone 12 Pro. IEEE Geosci Remote Sensing Lett. 19:1–5.
Kumar Karmacharya S, Bishwakarma M, Shrestha U, Rüther N. 2019. Application of "Structure from Motion" (SfM) technique in physical hydraulic modelling. J Phys: Conf Ser. 1266(1):012008.
Kuwata Y, Kawaguchi Y. 2019. Direct numerical simulation of turbulence over systematically varied irregular rough surfaces. J Fluid Mech. 862:781–815.
Lee CH. 2018. Rough boundary treatment method for the shear-stress transport k-x model. Eng Appl Comput Fluid Mech. 12(1):261–269.
Leonardi S, Orlandi P, Djenidi L, Antonia RA. 2006. Guidelines for modeling a 2D rough wall channel flow. Flow Turbulence Combust. 77(1–4):41–57.
Luetzenburg G, Kroon A, Bjørk AA. 2021. Evaluation of the Apple iPhone 12 Pro LiDAR for an application in geosciences. Sci Rep. 11(1):1–9.
Marteau B, Vericat D, Gibbins C, Batalla RJ, Green DR. 2017. Application of structure-from-motion photogrammetry to river restoration. Earth Surf Process Landforms. 42(3):503–515.
Masteller CC, Finnegan NJ. 2017. Interplay between grain protrusion and sediment entrainment in an experimen- tal flume. J Geophys Res Earth Surf. 122(1):274–289.
Monsalve A, Yager EM. 2017. Bed surface adjustments to spatially variable flow in low relative submergence regimes. Water Resour Res. 53(11):9350–9367.
Monsalve A, Yager EM, Schmeeckle MW. 2017. Effects of bedforms and large protruding grains on near-bed flow hydraulics in low relative submergence conditions. J Geophys Res Earth Surf. 122(10):1845–1866.
Morgan JA, Brogan DJ, Nelson PA. 2017. Application of structure-from-motion photogrammetry in laboratory flumes. Geomorphology. 276:125–143.
Nitsche M, Rickenmann D, Kirchner JW, Turowski JM, Badoux A. 2012. Macroroughness and variations in reach-averaged flow resistance in steep mountain streams. Water Resour Res. 48(12):W12518.
Paola C. 1985. A method for spatially averaging small- scale bottom roughness. Marine. 66(1–4):291–301.
Pearson E, Smith MW, Klaar MJ, Brown LE. 2017. Can high resolution 3D topographic surveys provide reliable grain size estimates in gravel bed rivers? Geomorphology. 293:143–155.
Poggi D, Porporato A, Ridolfi L. 2003. Analysis of the small-scale structure of turbulence on smooth and rough walls. Phys Fluids. 15(1):35–46.
Pokrajac D, Finnigan JJ, Manes C, McEwan I, Nikora V. 2006. On the definition of the shear velocity in rough bed open channel flows. In: Proceedings of the International Conference on Fluvial Hydraulics - River Flow 2006; p. 89– 98.
Roussinova V, Biswas N, Balachandar R. 2008. Revisiting tur- bulence in smooth uniform open channel flow. J Hydraulic Res. 46(sup1):36–48.
Schneider JM, Rickenmann D, Turowski JM, Bunte K, Kirchner JW. 2015. Applicability of bed load transport models for mixed-size sediments in steep streams con- sidering macro-roughness. Water Resour Res. 51(7): 5260–5283.
Schultz MP, Flack KA. 2009. Turbulent boundary layers on a systematically varied rough wall. Phys Fluids. 21(1):015104.
Smith MW, Carrivick JL, Quincey DJ. 2016. Structure from motion photogrammetry in physical geography. Prog Phys Geogr. 40(2):247–275.
Tabesh M, Hoffmann T, Vollmer S, Schüttrumpf H, Frings RM. 2019. In-situ measurement of river-bed sediment porosity using Structure-from-Motion image analysis. Geomorphology. 338:61–67.
Tavani S, Billi A, Corradetti A, Mercuri M, Bosman A, Cuffaro M, Seers T, Carminati E. 2022. Smartphone assisted fieldwork: towards the digital transition of geo- science fieldwork using LiDAR-equipped iPhones. Earth Sci Rev. 227:103969.
Tonina D, Jorde K. 2013. Hydraulic modelling approaches for ecohydraulic studies: 3D, 2D, 1D and non-numer- ical models. In: Maddock I, editor. Ecohydraulics: an integrated approach. Chichester, UK: John Wiley & Sons, Ltd; p. 31–74.
Vanderwel C, Ganapathisubramani B. 2019. Turbulent boundary layers over multiscale rough patches. Boundary-Layer Meteorol. 172(1):1–16.
Westoby MJ, Brasington J, Glasser NF, Hambrey MJ, Reynolds JM. 2012. Structure-from-motion" photogrammetry: a low-cost, effective tool for geoscience applications. Geomorphology. 179:300–314.
Woodget AS, Carbonneau PE, Visser F, Maddock IP. 2015. Quantifying submerged fluvial topography using hyperspatial resolution UAS imagery and structure from motion photogrammetry. Earth Surf Process Landforms. 40(1):47–64.